METRICA
METRology Institutional CAtalog

ISTITUTO NAZIONALE DI RICERCA METROLOGICA
Repository Istituzionale

Sprayable Ultrablack Coating Based on Hollow Carbon Nanospheres

This is the author's accepted version of the contribution published as:

Original
Sprayable Ultrablack Coating Based on Hollow Carbon Nanospheres / Hu, Yuefan; Cao, Kangli; Rong, Hao; Xu, Jun; Han, Hexiang; Wang, Huifen; Pattelli, Lorenzo; Li, Na; Xu, Hongbo; Zhao, Jiupeng; Pan, Lei; Kuchmizhak, Aleksandr; Li, Yao. - In: ACS APPLIED NANO MATERIALS. - ISSN 2574-0970. - 4:8(2021), pp. 7995-8002. [10.1021/acsanm.1c01291]

Availability:
This version is available at: 11696/71402 since: 2021-10-11T23:33:51Z

Publisher:
ACS Publications

Published
DOI:10.1021/acsanm.1c01291

Terms of use:

This article is made available under terms and conditions as specified in the corresponding bibliographic description in the repository

Publisher copyright
American Chemical Society (ACS)
Copyright © American Chemical Society after peer review and after technical editing by the publisher. To access the final edited and published work see the DOI above.

(Article begins on next page)

24 April 2024

Sprayable Ultra-Black Coating Based on Hollow Carbon Nanospheres

Yuefan Hu,[a] Kangli Cao,[b] Hao Rong,[a] Jun Xu,[b] Hexiang Han,[b] Huifen Wang,[b] Lorenzo Pattelli,[d,e] Na Li,[a] Hongbo Xu,[a] Jiupeng Zhao,[a] Lei Pan,[a,] Aleksandr Kuchmizhak,[f,g,*] and Yao Li[c,*]*

[a] MIIT Key Laboratory of Critical Materials Technology for New Energy Conversion and Storage, School of Chemistry and Chemical Engineering, Harbin Institute of Technology, Harbin, 150001, P. R. China

[b] Shanghai Institute of Spacecraft Equipment, Shanghai, 200240, P. R. China

[c] National Key Laboratory of Science and Technology on Advanced Composites in Special Environments, Harbin Institute of Technology, Harbin, 150001, China

[d] European Laboratory for Non-linear Spectroscopy (LENS), Università di Firenze, Sesto Fiorentino 50019, Italy

[e] Istituto Nazionale di Ricerca Metrologica (INRiM), 10135 Turin, Italy

[f] Institute for Automation and Control Processes, Far Eastern Branch, Russian Academy of Sciences, Vladivostok 690041, Russian Federation

[g] Far Eastern Federal University, Vladivostok 690922, Russia

Keywords: high absorption coatings; hollow carbon spheres; solar absorptance; adhesion; hierarchical structure

ABSTRACT: Inexpensive, easy-to-implement coatings exhibiting extremely low reflectance within a broad spectral range and good adhesion to substrates are in high demand for high-precision optical instruments and solar energy harvesting. Herein, we demonstrate a highly absorbing coating based on hollow carbon nanospheres (HCSs). The coatings are formed via a simple and high-performing air-spraying process with a tailored paint formulation containing HCSs as an absorbing pigment and a fluororesin as a binder. By optimizing the pigment/binder mass ratio (P/B), we produce functional coatings that exhibit solar absorptance up to 0.985 and good adhesion to aluminum sheets of grade 2 (according to the ISO 2409 standard). The excellent solar absorptance of the obtained coatings results from their hierarchical nano- and micro-scale surface morphology, providing a refractive index gradient on the air-coating interface as well as

remarkable light trapping performance. The former is due to the hollow structure in carbon spheres, which is preserved after the addition of the binder because the size of binder particles is larger than the holes on the shell of the HCSs. The latter is attributed to the micro-nodules and micro-pits of the coating surface formed by the agglomeration of the HCSs, which enhances absorption by multiple scattering.

1. Introduction

As predicted by Snell's law, reflection occurring at the air-solid interface is inevitable due to the presence of a refractive index discontinuity. Unwanted reflections are detrimental for many applications such as high-performance optical devices or solar energy collectors.[1,2] In these cases, "ultra-black" surfaces possessing extremely low reflectance over a broad spectral range are highly demanded.

Numerous studies were undertaken to minimize the surface reflection.[3,4] In general, three basic principles, operating independently or simultaneously,[5] have been employed to form a natural[6, 7] or artificially designed low-reflectivity surface in these studies:

(1) Formation of large (as compared to the wavelength) nodules or pits to trap incident light via multiple reflections and absorptions within the surface;[8-15]

(2) Incorporation of low-density surface layers to produce a gradual variation of the refractive index, suppressing Fresnel reflection;[9,15-23]

(3) Use of noble-metal or high-refractive-index nanoparticles to achieve efficient broadband solar absorption via bandgap engineering or by coupling to either surface plasmons or Mie-type resonances.[4,24-27]

Carbon is the most commonly used absorber for black paints due to its low price and wide absorption band. Carbon-based materials with low density such as carbon nanotubes have been widely employed as ultra-black materials for high-end optical applications. Yang et al. obtained an extremely low reflectance (lower than 0.07%) within a visible wavelength range of 457-633 nm using arrays of aligned nanotubes produced by a chemical vapor deposition.[18] Zhu et al. fabricated carbon aerogels via a supercritical drying method, which exhibited a total reflectance lower than 0.24% in a spectral range of 400-2000 nm.[19] Mentioned materials demonstrated an excellent light-absorbing performance due to multiple open pores, which decrease the refractive index jump at the air interface. However, the produced coatings typically had weak adhesion to a substrate or were prepared in the form of a self-supporting membrane, thus limiting their practical applicability. To improve the adhesion of the nanotube-based coatings, Magdassi et al. mixed multi-walled

carbon nanotubes with a silicone, then the mixture was sprayed on an aluminum substrate to obtain the ultra-black coating.[28-30] The resulting adhesion was significantly improved, but at the cost of a substantial increase of average reflectance up to 2-5%, i.e. to a level that is not acceptable for certain applications. Similar result is reported for carbon aerogels[31] too. This is due to the fact that the binder infiltrates the gaps between the nanotubes potentially penetrating into the nanotubes, as well. Negative contribution of the binder can be mitigated by reducing its concentration, for example, by using tightly packed nanoparticles or introducing empty closed-cell pores[32] to obtain a smoother refractive index transition at the air-coating interface.

In this study, we report the fabrication of ultra-black coatings based on hollow carbon nanospheres (HCSs), which were chosen as an absorbing pigment according to the following reasons. First of all, the hollow structure of the nanospheres reduces the overall density and average refractive index of the resulting coatings. Second, the agglomerated HCSs create a disordered micro-scale surface morphology that facilitates light trapping and reduces inter-particle gaps, decreasing the binder consumption. Figure 1 schematically illustrates the general structure of the proposed HCS-based coating. The agglomerated hollow spheres form micron-sized surface nodules and pits wrapped by a thin binder layer which fills the inter-particle gaps, while the hollow

core remains intact. When light irradiates such a hierarchical surface, reflection is substantially suppressed via light trapping and decreased Fresnel reflection.

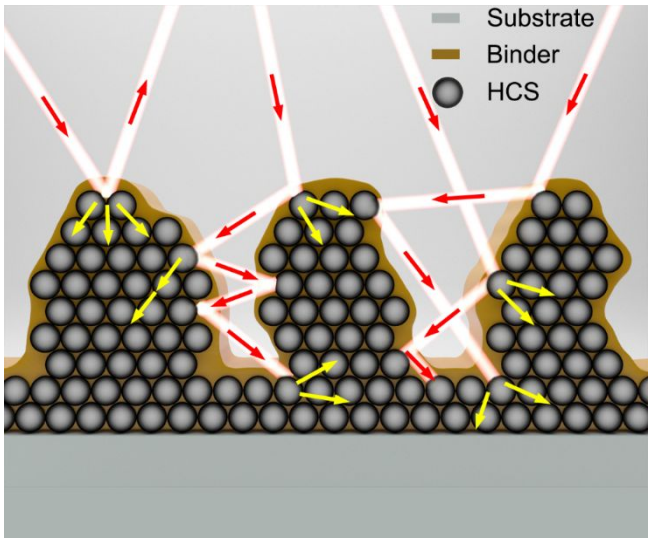

Figure 1. Schematic of the proposed HCS-based coating. The incident light rays in the air are shown by red arrows, while the yellow ones indicate the radiation trapped by the HCSs.

2. Experimental Section/Methods

2.1 Chemicals and materials

Analytical grade reagents including ammonia, ethyl alcohol, resorcinol, formaldehyde, cetyltrimethylammonium bromide (CTAB), hydrofluoric acid and acetone were purchased from Sigma-Aldrich and used without further purification. Poly(vinylidene fluoride-*co*-

chlorotrifluoroethylene) was purchased from HWRK CHEM (China) and used as a binder. Tetraethyl orthosilicate (TEOS) was distilled before use. Ultra-pure water was obtained from an in-house filtration system (CSR-1-30T).

2.2 Preparation of HCSs

HCSs were synthesized according to the methods described in the literature.[33-35] The process involves four steps: (1) the synthesis of SiO_2 spherical particles, (2) their coating by the resorcinol formaldehyde resin (RF resin), (3) carbonization of SiO_2@RF spheres, and (4) the removal of the remaining SiO_2 via etching (Figure 2).

Figure 2. Schematic of the HCS synthesis

(1) Synthesis of silica microspheres as a sacrificial template. First, 22 mL water, 150 mL ethanol, and 9 mL ammonium solution (14 mol/L) were mixed in a 500 mL reactor in a water bath at 40℃ and vigorously stirred for 5 min. Then, 5 g TEOS and 20 ml ethyl alcohol were added into the

reactor. A colloidal solution of SiO_2 nanospheres with a diameter of approximately 150~200 nm was obtained by maintaining the temperature and stirring for 8 h.

(2) Synthesis of RF-resin-coated SiO_2 spheres. 2 g of SiO_2 spheres were washed twice and mixed with 3 mL of ammonia solution (14 mol/L) and 20 mL of CTAB (0.01 mol/L) in 500 mL of water in a 1L reactor, followed by stirring for 5 min. Subsequently, 2 g resorcinol and 25 mL (40% volume) of formaldehyde solution were added in the reactor. The SiO_2@RF composite was obtained after stirring at room temperature for 15 h.

(3) Synthesis of carbon-coated SiO_2 spheres. After a series of precipitation, washing and drying steps, the SiO_2@RF composite was heated at 600 ℃ under an Ar atmosphere for 8 h to obtain the clumped SiO_2@C.

(4) Synthesis of hollow carbon sphere. SiO_2@C was further ground into powder using a mortar. Then, the powder was etched in HF solution under vigorous stirring to remove SiO_2, leaving only the carbon shell. After drying, the HCSs was ground again to improve dispersion in the fluororesin solution.

2.3 Preparation of the HCS coating

An aluminum sheet was roughened by sandpaper and used as a substrate for HCS-based coatings. The typical roughness of the Al sheet assessed using optical profilometry was about 3 μm (Figure S1). The paint was prepared by mixing the HCSs with the fluororesin in acetone at different ratios and sonicated for 10 min. Then the paint was uniformly sprayed onto the Al sheets by an air spraying gun. Typically, spraying procedure was repeated several times to achieve uniform coverage (see Supporting Information). Finally, the coatings were put at room temperature for 30 min until complete solidification.

2.4 Coating characterization

The surface morphology of the produced coatings was studied by a field-emission scanning electron microscope (Hitachi SU 8010) and transmission electron microscope (Hitachi H-7650). Reactive ion etching (RIE) of the HCS coatings was performed with a RIE apparatus (RIE-601) using argon as the reactive gas, that allowed to etch both the HCSs and the fluororesin. Etching depth was controlled by varying the etching time. The working power, reactor pressure and argon flow rate were set to 150 W, 100 mtorr, and 30 sccm, respectively.

The solar absorptance, A_s, was calculated from the diffuse reflection spectra measured by the Lambda 950 UV-visible spectrophotometer coupled to an integrating sphere. Since the coatings

were applied above the Al substrates, the total transmittance is zero (T_s=0), and the solar absorptance can be assessed as:

$$A_s = 1 - R_s \quad (1)$$

where R_s is the solar reflectance defined as the ratio between reflected and incident solar flux. Reflectance of the HCS-based coatings was also modeled using finite-difference time-domain (FDTD) calculations (Figure S2). The 5-μm thick coatings comprised of the randomly arranged monodisperse HCSs with variable diameter and shell thickness were simulated. The simulation volume was limited by periodic boundary conditions applied along both lateral directions as well as perfect matched layers along vertical direction.

Nitrogen adsorption was used to estimate the pore size distribution and pore volume of materials by measuring the amount of the gas condensed on the sample at variable pressure. The size of fluororesin molecule was assessed using dynamic light scattering (DLS, Malvern Zetasizer nano ZS90).

Adhesion of the HCS coatings was evaluated according to the ISO 2409 standard. Specifically, HCS coatings were cut horizontally and vertically at a distance of 1 mm and stuck with a tape several times to classify the fraction of detached material according to a standard scale.

3. Results and discussion

3.1 HCS-based coatings: key factors of high absorptance

As mentioned above, the synthesis of the HCSs involves four consecutive steps. Figure 3 demonstrates evolution of the morphologies of the SiO_2 nanospheres obtained at each step. It can be observed that the initial diameter of the SiO_2 nanospheres is approximately 170 nm (Figure 3a), which ensures the subwavelength size of the resulting HCS product. Figure 3b,c demonstrates the morphologies of the SiO_2@RF and SiO_2@C nanospheres, respectively. Both these products show partial agglomeration, leading to the formation of micron-sized surface features. SEM and TEM images of the final product reveal hollow structure of the carbon nanospheres, particularly owing to appearance of nanospheres with a broken shell (Figure 3d,e). The break of the shell may result from the grinding process of the partially agglomerated nanomaterial; however, the majority of the HCSs preserve unbroken shell. In this respect, the broken nanospheres are expected to weakly affect the optical properties of the resulting HCS-based coatings. Noteworthy, the average size of the HCSs reduces down to 153 nm with respect to 170-nm diameter pristine SiO_2 nanospheres. This is caused by the shrinkage of SiO_2[36] and the carbon sphere during the calcination process.

According to the performed TEM studies the thickness of the carbon shell is about 14 nm (Figure 3e, inset).

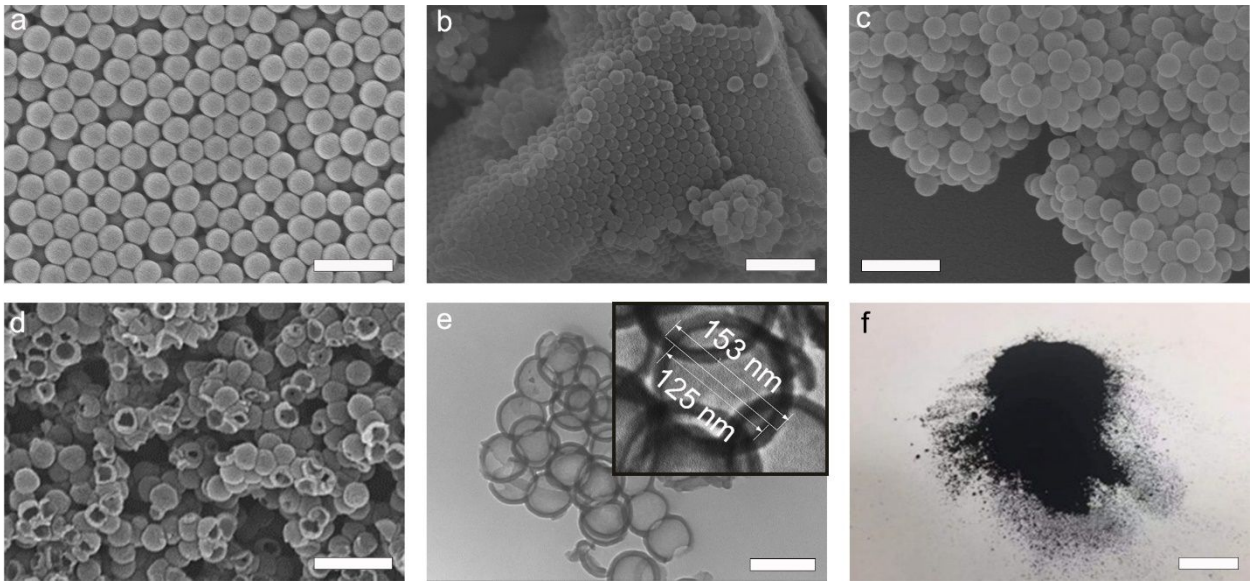

Figure 3. (a-d) Series of SEM images showing the evolution of the morphology of the SiO_2 microspheres on each consecutive fabrication step. (e) TEM image of the produced HCSs. Inset provides magnified view of representative nanosphere with the outer and inner diameters around 153 and 125 nm yielding in the corresponding average carbon shell thickness of 14 nm. (f) Optical image of the HCS-based powder. The scale bars in the images (a)-(f) correspond to 500 nm, 1 μm, 500 nm, 500 nm, 200 nm, 2 cm respectively.

As recently reported by Guo *et al.*, HCSs as spherically symmetric structures exhibit geometry-dependent scattering resonances that selectively enhance reflectance at certain wavelengths and lead to conspicuous coloration of the HCS-based coatings.[37] However, our HCS powders appear completely black (Figure 3f), which can be ascribed to the smaller size of the used nanospheres with respect to those reported in [37]. This deduction was particularly confirmed by numerical modeling of the reflectance spectra of the HCS-based coatings containing several layers of randomly arranged HCSs with different diameters (Figure S2). As expected, the reflectance peaks observed in the calculated spectra demonstrate systematic blueshift at decreasing diameter of the HCSs, moving out of the solar wavelength range when the diameter of HCSs reaches 150 nm. As we will show further, this is well consistent with the measured spectral response of the HCS-based coatings. Therefore, in our case, the spherical symmetry of the used HCSs does not represent a problem, allowing to obtain highly absorbing nanomaterial via simple synthesis procedure. Noteworthy, utilization of the polydisperse HCSs can potentially solve the problem associated with a structural color that comes from the spherical symmetry of the nanoparticles. For example, this can be easily achieved by using TEOS with low purity. However, apart from expectedly low

reproducibility of the produced coatings, polydisperse HCSs cannot provide the densest arrangement that will require more binder and result in higher reflectance of the produced coatings.

The paint solutions were prepared by mixing the HCSs with the fluororesin binder at different mass ratio (P:B) and air-sprayed on the Al sheets. Noteworthy, the binder concentration strongly affects the spraying process. At a specific P:B ratio, a lower binder concentration results in higher amount of the used solvent and lower viscosity of the resulting solution. When the viscosity is too low, the fluidity of the liquid drops on the Al sheet is too high, which is not conducive to the formation of uniform coating, especially at the non-horizontal surface. However, if the viscosity is too high, the risk of clogging of the spray gun increases. Therefore, we chose the range of the binder concentrations at which spraying can be carried out safely. At such concentrations, because the fluidity of the droplets is very low, spraying procedure are to be performed several times to produce uniform HCS-based coating completely covering the Al sheet (Figure S3). The minimal thickness of such uniform coating was assessed to be about 30 μm (Figure S4).

Integral reflectance R_s of the HCS-based coatings produced at different P/B ratio was systematically measured across the wavelength range of 250-2500 nm. These measurements showed that the coating reflectance increases with the binder content (Figure 4). More specifically,

when P/B is 1:10, the integral solar absorptance A_s is 0.963 (R_s=0.037), reaching 0.985 (R_s=0.015) at P/B=1:2. Further decrease of the binder content leads to a visible reduction of the adhesion of the produced coatings. The variation of the solar absorptance with the binder amount is associated to a corresponding evolution of the morphology of the produced HCS-based coatings. In particular, Figure 5a,b shows that the surface of the black coating produced at P/B of 1:10 exhibits rather gentle protrusions insufficient to provide significant light trapping performance. Furthermore, HCSs can hardly be identified beneath the coating surface, indicating an excessive amount of the binder. This leads to an increased refractive index contrast at the air–coating interface. In contrast, the rough surface of the coating produced at P/B of 1:2 is characterized by multiple micron-scale pits made of agglomerated nanospheres where light can penetrate and undergo multiple scattering and absorption events (see Figure 5c). A closer look at the surface morphology of such coating shows agglomerated HCSs capped by a thin resin "skin" (Figure 5d), which favors suppression of the Fresnel reflection and facilitates the absorption of the incident light. Both the rough surface morphology and the relative increase of the pigment mass content contribute to the strong integral absorptance of the HCS-based coatings produced at P/B = 1:2. In this respect, it is complicated to assess contribution of both factors to the achieved low solar absorptance. Noteworthy, as it was

mentioned above, the minimal thickness of the uniform HCS-based coating was about 30 μm. Further increase of the coating thickness provided no evident improvement of the integral solar absorptance, while required excessive usage of the nanomaterial and chemicals.

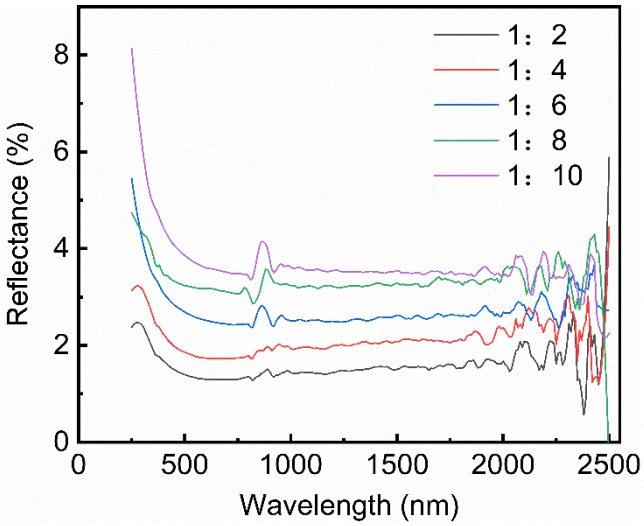

Figure 4. Reflectance spectra of the HCS-based coatings produced at different P/B mass ratio.

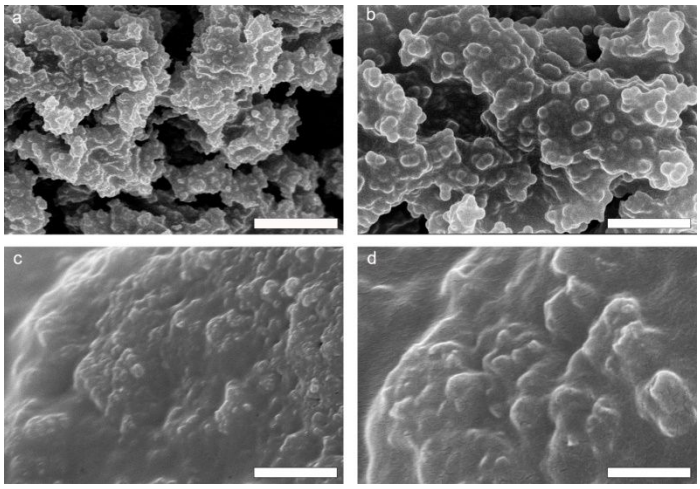

Figure 5. SEM images illustrating morphology of the HCS-based coatings with a P/B ration of 1:2 (a,b) and 1:10 (c,d). The scale bars correspond to 5 μm in (a,c), and 500 nm in (b,d).

To clarify the effect of the hollow microsphere geometry on the absorption characteristics of the HCS-based paints, we fabricated and tested the additional type of coating made of solid carbon sphere (SCS) mixed with a binder at similar P/B ratio (see Figure S5). Similarly to the HCS-based coatings, the averaged reflectance of the SCS-based coatings increases at elevated binder content as it is illustrated in Figure 6. The strongest solar absorptance of 0.978 (R_s=0.022) was achieved at P/B ratio of 1:1. Noteworthy, such coating possesses physical characteristics and surface morphology close to those for the HCS-based coating produced at P/B ratio of 1:2 (see Figure S6). Meanwhile, difference in the achieved averaged reflectance for both coatings clearly reveals the positive effect of the hollow morphology of the nanospheres on light-absorbing performance of the resulting coating. At first glance, the difference between HCS- and SCS-based coatings may seem insignificant; however, for certain applications as stray light suppression, such improvement will play crucial role in resulting device performance. For example, when the stray light hits the

black-covered hood for 10 subsequent reflections, the HCS coating will provide 46-fold stronger suppression of the reflected light intensity compared to that of the SCS-based coating.

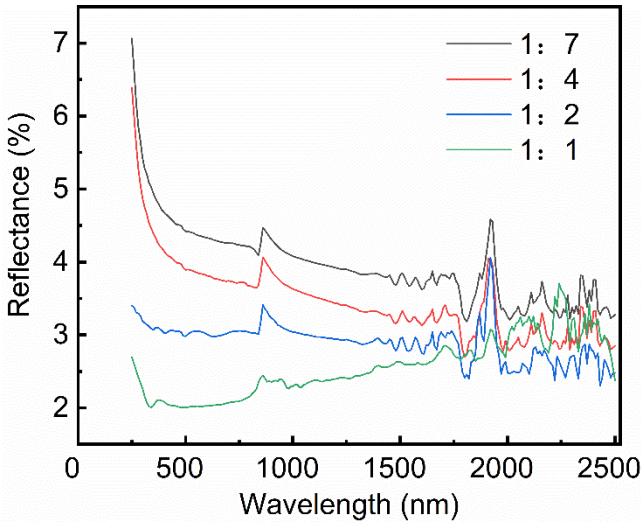

Figure 6. Reflectance spectra of the SCS-based coatings produced at different P/B ratio.

3.2 Preservation of hollow morphology of the nanospheres mixed with a binder

To ensure the highest absorption, the HCSs must preserve hollow morphology when mixed with a binder to produce the ultra-black coating. However, the fluororesin can potentially penetrate inside the HCSs through the nanopores formed in the carbon shell of the HCSs during calcination process (Figure 2). RIE procedure was first carried out to reveal internal structure of the HCSs in the produced coatings. The surface morphology of the HCS-based coating (with P/B ratio of 1:2) etched at different depths by varying exposure time from 2 to 10 min is illustrated by a series of

SEM images in Figure 7. As can be seen, no visible blockage is detected inside the isolated HCSs visualized at different etching stages confirming impermeability of the carbon shells.

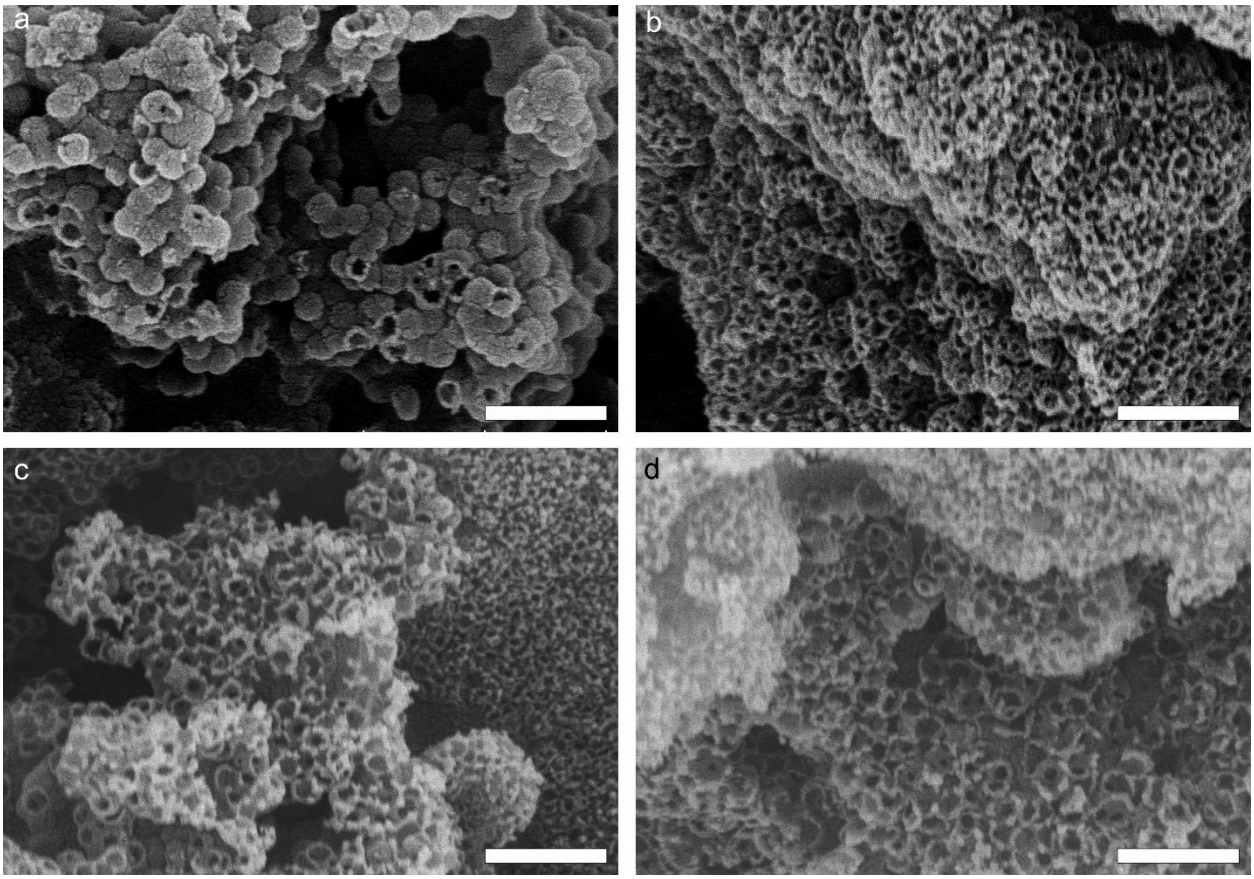

Figure 7. Series of SEM images showing surface morphology of the HCS-based coatings after their reactive ion etching at different etching time: 2 min (a), 4 min (b), 6 min (c) and 10 min (d). The scale bars are 500 nm for all images.

To further explore why fluororesin does not penetrate into the HCSs, the distribution of the pore size in the carbon shell were examined using nitrogen adsorption method. The N_2 adsorption-

desorption isotherms of the HCSs (Figure 8a) shows a sharp capillary condensation at high partial pressure (p/p_0=0.91-0.99; p is the pressure at equilibrium, p_0 is the saturated vapor pressure) as well as H1-type hysteresis loop, indicating a narrow pore size distribution. At low partial pressure (p/p_0<0.4), the adsorption and desorption curves are very close, indicating the presence of the multiple nanopores. The relationship between differential pore volume ($\Delta V/\Delta W$) and pore size (W) was obtained through the Density Functional Theory. As shown in Figure 8b, the HCSs show a bimodal pore distribution. The main maximum at 120.8 nm can be attributed to the hollow core of the HCSs, while the second one (around 1 nm) – to the nanopores in the carbon shell. Approximate size of the fluororesin particles was evaluated using DLS and Tyndall test (Figures S7 and S8). DLS measurements indicated hydrodynamic feature size of the fluororesin of about few hundred nanometers, that could correspond to one-dimensional size of the unfold fluororesin chain. Distinct laser radiation path observed during the Tyndall test also confirmed similar characteristic size of the fluororesin. The difference in the characteristic size of the shell nanopores and the fluororesin apparently explains the impermeability of the carbon shell.

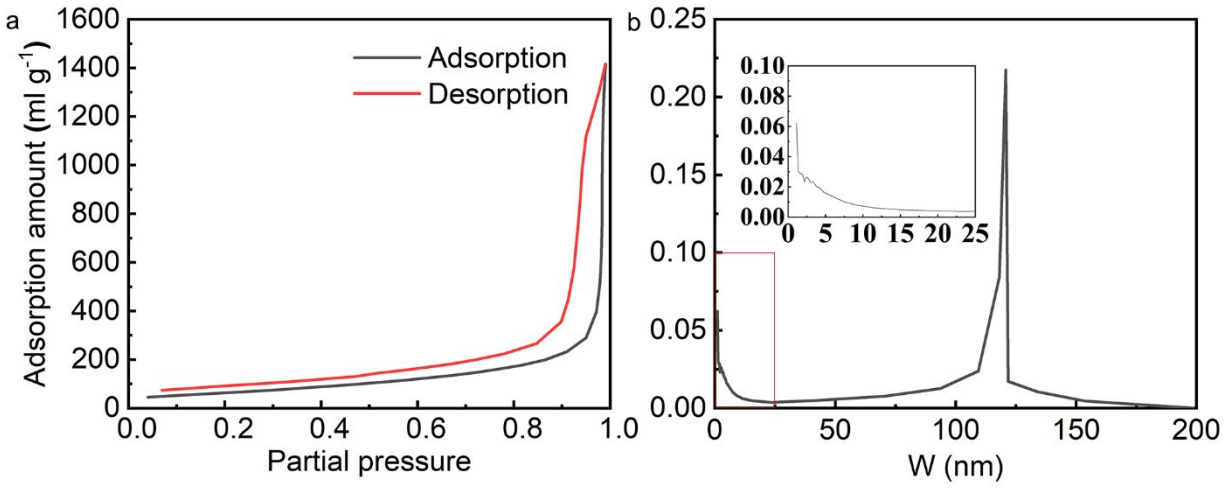

Figure 8. (a) Adsorption-desorption isotherm of nitrogen with respect to the HCS; (b) Differential pore volume ΔV/ΔW as a function of the pore size W calculated by the Density Functional Theory. Inset shows a magnified view of the red-square area.

3.3 Adhesion of the HCS-based coatings

The adhesion of the ultra-black coatings to the substrates is essential for practical applications. The adhesion of the HCS-based coatings produced at different P/B ratio was evaluated by the standard cross-cut tape test (ISO 2409). Figure 9 provides optical photograph of the coatings arranged on a black cloth after performing adhesion test. Reflectance spectrum of the black cloth is provided in Figure S9. As can be seen, the HCS-based coatings with high binder content (P/B ratio of 1:8 and 1:10) demonstrate remarkable adhesion characterized by small detached areas only

near the cut intersections. This results can be used to rate such coatings as grade 1. The coatings produced at moderate P/B ratio of 1:6 and 1:4 shows detached areas not only at the intersection but also along the cut edges. Nonetheless, the affected cross-cutting area was less than 15%, and the adhesion of such coatings can be rated as grade 2. For HCS-based coatings with the highest absorbance (P/B ratio of 1:2), their adhesion was rated as grade 3 according to the affected cross-cutting area less than 35% making such coatings of practical interest as well. At even higher P/B ratios, such as 1:1, the adhesion becomes too weak leading to large-area peeling of the coating material even when it is subjected to slight scratches.

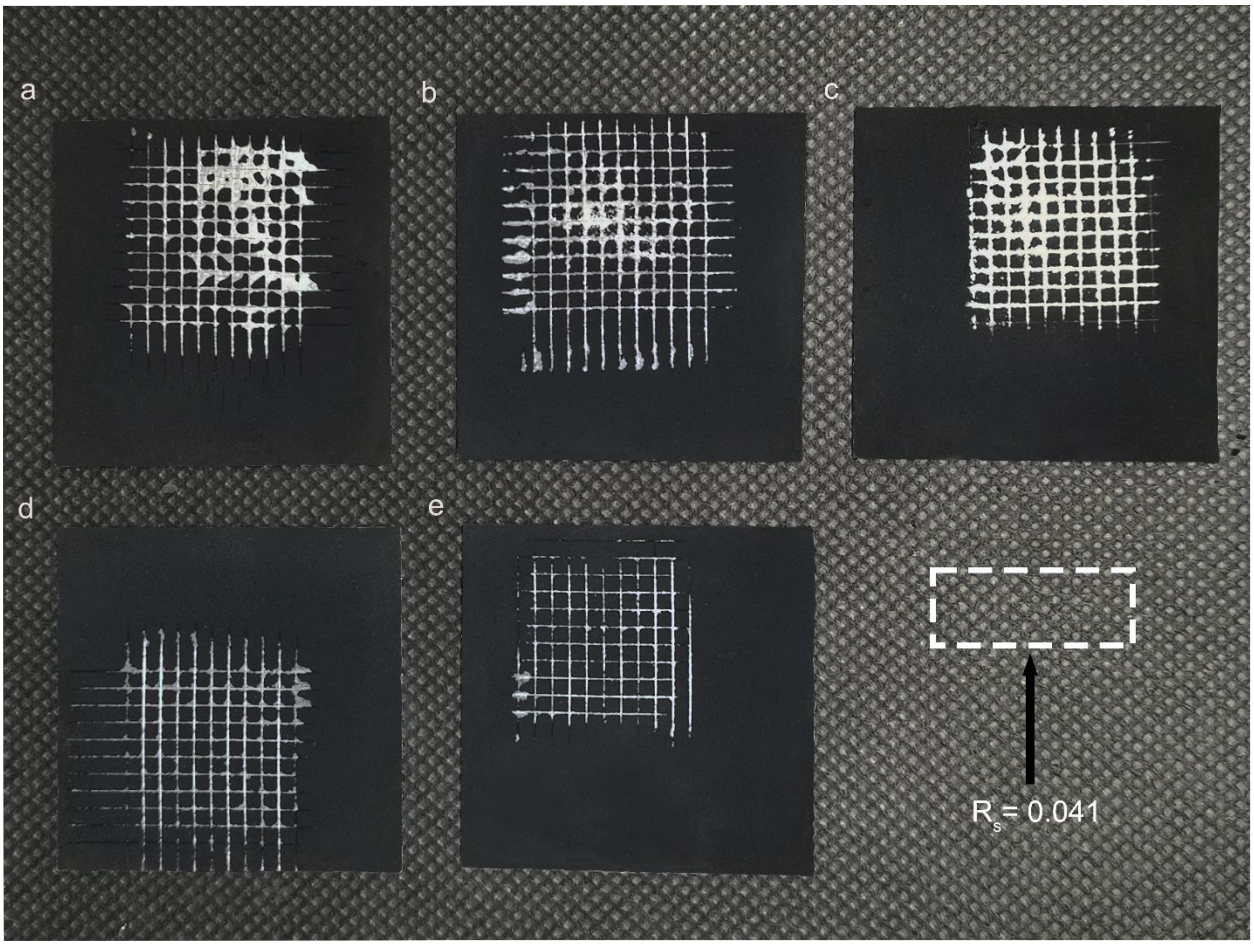

Figure 9. Digital images of the HCS-based coatings produced at different P/B ratio after performing the standard adhesion tests on a black paper. The black paper with solar reflectance of 0.041 is used as the background. The P/B ratio is (a) 1： 2; (b) 1:4; (c) 1:6; (d) 1:8; (e) 1:10. The length of a lattice with a white border is 2 mm.

Finally, to highlight the importance of the obtained results, we compare the main relevant characteristics of several reported state-of-the-art ultra-black carbon-based coatings with those

obtained for the developed HCSs-based coatings (Table 1). Pure (or binder-free) low-density carbon-based materials typically provide integral absorption better than 0.99. However, these characteristics decrease significantly (ca. 0.02) when the nanomaterial is mixed with the binder that is required to achieve strong adhesion to the substrate in realistic applications.[28-30] Similar idea is clearly illustrated in Supporting Movie showing the reflectivity of He-Ne laser from several ultra-black coatings. Conversely, the integral absorptance of the HCS-based coatings maintains a high value of 0.985. This direct comparison indicated that the innovative HCS-based coatings provide an excellent trade-off between strong broadband light absorption and good adhesion to the substrate.

Table 1. The light absorption and adhesion performance of ultra-black carbon-based nanomaterials

ultra-black materials	Optical property		Adding binder	Adhesion	Refs.
	spectrum range (nm)	integral absorptance			
Graphite nanocone nanowire composite	400-2000	ca 0.995	No	\	[16]
Hierarchical porous carbon spheres	300-2000	＞0.997	No	\	[13]

Carbon aerogel	400-2000	＞0.997	No	\	[19]
Carbon Vesicles	250-2000	>0.998	No	\	[37]
Carbon aerogel	400-1100	ca 0.98	Yes	grade 0	[31]
Multiwalled carbon nanotubes (MWCNT)	350-800 850-2400	ca 0.973 ca 0.961	Yes	grade 3	[28]
AlOOH/MWCNT	300-2500	ca 0.975	Yes	grade 1	[29]
Hollow carbon spheres	250-2500	0.985	Yes	grade 2 and 3	this work *

4. Conclusion

In this study, coatings with excellent solar absorptance were successfully fabricated by a simple and high-performing air-spraying process with a specially designed paint containing HCSs as a pigment and a fluororesin as a binder. By optimizing the pigment/binder ratio (P/B), a maximum solar absorptance of 0.985 was obtained at P/B of 1:2. Reactive ion etching proved the hollow nano-morphology of the HCSs that was preserved after the curing process. Tyndall effect, dynamic light scattering and nitrogen adsorption were used to assess and compare the typical size of the fluororesin particle and nanopore in the HCS shell explaining why the former can't penetrate inside the HCSs. The presence of hollow nanospheres allows to reduce the overall density of the coatings,

thus decreasing the Fresnel reflection, while the micro-scale surface morphology formed by the agglomerated HCSs favors multiple reflections facilitating light absorption. In addition to remarkable light absorption performance, good adhesion of the ultra-black coating to a substrate is mandatory for practical application, which can be achieved by using a binder. However, the addition of a binder typically causes a substantial increase of the averaged reflectance. In this work, we have optimized the pigment/binder ratio and spraying procedure to achieve the coating maintaining a strong absorbance combined with satisfactory good adhesion (grade 2 and 3 according to the ISO 2409 standard). Demonstrated characteristics make the produced HCS-based coatings suitable for realistic applications such as solar energy harvesting, photothermal conversion and designing of high-precision optical instruments. Moreover, the produced ultra-black coatings possess rather low reflectance in the mid-IR spectral range (see Figure S10). This indicates their high thermal emittance that is helpful for the temperature balance of the optical instrument designed for space applications.

It should be stressed out that small amount of the hollow nanospheres appears to have a broken shell after the grinding process. This can cause a certain increase of the reflectivity owing to penetration of the binder inside the broken nanospheres. In this respect, further optimization of the

fabrication procedures can potentially improve light absorbing characteristics without reducing adhesion performance. Nanospheres with more complicated multi-layer morphology can be also considered as promising way to improved light absorption characteristics of the black paint[15,38]. However, additional studies are to be implemented to evaluate their matching with a binder to realize coating with good adhesion. Such aspects as mixing ratio and potential penetration of binder molecules inside the multi-layer nanospheres should be studied carefully to make the decision regarding their capability to improve the already obtained characteristics. Other factors as final price of the black paint and are also relevant for realistic applications.

ASSOCIATED CONTENT

Supporting Information

The following files are available free of charge.

Figure S1: Microtopography of the roughened Al sheet; Figure S2: Calculated reflectance of the HCS-based coatings made of carbon nanospheres of variable outer diameter and shell thickness

Figure S3: Optical photograph of the HCS-based coatings produced by performing spraying procedure several times; Figure S4: Side-view SEM images of the HCS-based coatings; Figure S5: Comparative optical images of SCS- and HCS-based coatings; Figure S6: . Representative

SEM images demonstrating the surface morphology of the SCS-based coating; Figure S7: Dynamic light scattering measurements of fluororesin; Figure S8: Tyndall effect in the fluororesin solution; Figure S9: Reflection spectra of the black cloth; Figure S10: Reflectance of ultra-black coating in thermal emittance band; Supplementary video comparing the He-Ne laser reflection from different ultra-black coatings (MP4)

AUTHOR INFORMATION

Corresponding Author

Lei Pan — MIIT Key Laboratory of Critical Materials Technology for New Energy Conversion and Storage, School of Chemistry and Chemical Engineering, Harbin Institute of Technology, Harbin, 150001, P. R. China;

E-mail: panlei@hit.edu.cn

Aleksandr Kuchmizhak — Institute for Automation and Control Processes, Far Eastern Branch, Russian Academy of Sciences, Vladivostok 690041, Russian Federation; Far Eastern Federal University, Vladivostok 690922, Russia;

E-mail: alex.iacp.dvo@mail.ru

Yao Li — National Key Laboratory of Science and Technology on Advanced Composites in Special Environments, Harbin Institute of Technology, Harbin, 150001, China;

E-mail: yaoli@hit.edu.cn

Authors

Yuefan Hu, Hao Rong, Na Li, Hongbo Xu, Jiupeng Zhao — MIIT Key Laboratory of Critical Materials Technology for New Energy Conversion and Storage, School of Chemistry and Chemical Engineering, Harbin Institute of Technology, Harbin, 150001, P. R. China

Kangli Cao, Jun Xu, Hexiang Han, Huifen Wang — Shanghai Institute of Spacecraft Equipment, Shanghai, 200240, P. R. China

LorenzoPattelli — European Laboratory for Non-linear Spectroscopy (LENS), Università di Firenze, Sesto Fiorentino 50019, Italy;Istituto Nazionale di Ricerca Metrologica (INRiM), 10135 Turin, Italy

Notes

The authors declare no competing financial interest.

ACKNOWLEDGMENTS

This work was supported by Shanghai Aerospace Science and Technology Innovation Fund (SAST2017-065), Heilongjiang Provincial Postdoctoral Science Foundation (LBHZ-15078, LBHZ-16080), China Postdoctoral Science Foundation (2016M601427) and National Natural Science Foundation of China (No.51761135123, 52072096). A.K. expresses his gratitude to the Ministry of Science and Higher Education of the Russian Federation (Grant Nos. MK-4321.2021.1.2).

ABBREVIATIONS

HCS, hollow carbon sphere; P/B, pigment binder mass ratio; SCS, solid carbon sphere

REFERENCES

(1) Persky, M. J., Review of black surfaces for space-borne infrared systems. *Rev. Sci. Instrum.* **1999**, 70, 2193-2217.

(2) Mccall, S. H. C. P.; Pompea, S. M.; Breault, R. P.; Regens, N. L., Reviews of Black Surfaces for Space and Ground-Based Optical-Systems. In *Stray Radiation in Optical Systems II 1993*, *Proceedings of the Society of Photo-Optical Instrumentation Engineers,* San Diego, California, July 20-22,**1992**.

(3) Dou, S. L.; Xu, H. B.; Zhao, J. P.; Zhang, K.; Li, N.; Lin, Y. P.; Pan, L.; Li, Y., Bioinspired Microstructured Materials for Optical and Thermal Regulation. *Adv. Mater.* **2020**, DIO:10.1002/adma.202000697.

(4) Huang, J. F.; Liu, C. X.; Zhu, Y. H.; Masala, S.; Alarousu, E.; Han, Y.; Fratalocchi, A., Harnessing structural darkness in the visible and infrared wavelengths for a new source of light. *Nat. Nanotechnol* **2016**, 11, 60.

(5) Fan, P. X.; Bai, B. F.; Jin, G. F.; Zhang, H. J.; Zhong, M. L., Patternable fabrication of hyper-hierarchical metal surface structures for ultrabroadband antireflection and self-cleaning. *Appl. Surf. Sci.* **2018**, 457, 991-999.

(6) Niu, S. C.; Li, B.; Mu, Z. Z.; Yang, M.; Zhang, J. Q.; Han, Z. W.; Ren, L. Q., Excellent structure-based multifunction of morpho butterfly wings: a review. *J. Bionic Eng.* **2015**, 12, 170-189.

(7) Han, Z. W.; Li, B.; Mu, Z. Z.; Yang, M.; Niu, S. C.; Zhang, J. Q.; Ren, L. Q., An ingenious super light trapping surface templated from butterfly wing scales. *Nnaoscale Res. Lett.* **2015**, 10, 334.

(8) Han, Z. W.; Niu, S. C.; Li, W.; Ren, L. Q., Preparation of bionic nanostructures from butterfly wings and their low reflectivity of ultraviolet. *Appl. Phys. Lett.* **2013**, 102,233702.

(9) Zhao, Q. B.; Fan, T. X.; Ding, J. A.; Zhang, D.; Guo, Q. X.; Kamada, M., Super black and ultrathin amorphous carbon film inspired by anti-reflection architecture in butterfly wing. *Carbon* **2011**, 49, 877-883.

(10) Fan, P. X.; Bai, B. F.; Zhong, M. L.; Zhang, H. J.; Long, J. Y.; Han, J. P.; Wang, W. Q.; Jin, G. F., General Strategy toward Dual-Scale-Controlled Metallic Micro-Nano Hybrid Structures with Ultralow Reflectance. *Acs Nano* **2017**, 11, 7401-7408.

(11) Yao, Z. P.; Hu, B.; Shen, Q. X.; Niu, A. X.; Jiang, Z. H.; Su, P. B.; Ju, P. F., Preparation of black high absorbance and high emissivity thermal control coating on Ti alloy by plasma electrolytic oxidation. *Surf. Coat. Tech.* **2014**, 253, 166-170.

(12) Xing, F.; Zhao, B. R.; Shi, W. Y., Study on tunable fabrication of the ultra-black Ni-P film and its blacking mechanism. *Electrochim. Acta.* **2013**, 100, 157-163.

(13) Guo, J.; Li, D. D.; Zhao, H.; Zou, W. Z.; Yang, Z. S.; Qian, Z. C.; Yang, S. J.; Yang, M.; Zhao, N.; Xu, J., Cast-and-Use Super Black Coating Based on Polymer-Derived Hierarchical Porous Carbon Spheres. *Acs Appl. Mater. Inter.* **2019**, 11, 15945-15951.

(14) Xu, H. B.; Lu, N.; Qi, D. P.; Hao, J. Y.; Gao, L. G.; Zhang, B.; Chi, L. F., Biomimetic Antireflective Si Nanopillar Arrays. *Small* **2008**, 4, 1972-1975.

(15) Carlesso, F.; Vieira, L. E. A.; Berni, L. A.; Savonov, G. d. S.; Oliva, A. R.; Finsterle, W.; de Miranda, E. L., Physical and Optical Properties of Ultra-black Nickel-Phosphorus for a Total Solar Irradiance Measurement. *Astrophysical Journal Supplement Series* **2020,** *248* (1).

(16) Sun, Y. R.; Evans, J.; Ding, F.; Liu, N.; Liu, W.; Zhang, Y.; He, S. L., Bendable, ultra-black absorber based on a graphite nanocone nanowire composite structure. *Opt. Express* **2015**, 23, 20115-20123.

(17) Sun, C. H.; Jiang, P.; Jiang, B., Broadband moth-eye antireflection coatings on silicon. *Appl. Phys. Lett.* **2008**, 92,061112.

(18) Yang, Z. P.; Ci, L. J.; Bur, J. A.; Lin, S. Y.; Ajayan, P. M., Experimental observation of an extremely dark material made by a low-density nanotube array. *Nano Lett.* **2008**, 8, 446-451.

(19) Zhu, J. Y.; Yang, X.; Fu, Z. B.; Wang, C. Y.; Wu, W. D.; Zhang, L., Facile fabrication of ultra-low density, high-surface-area, broadband antireflective carbon aerogels as ultra-black materials. *J. Porous. Mat.* **2016**, 23, 1217-1225.

(20) Sun, W.; Du, A.; Feng, Y.; Shen, J.; Huang, S. M.; Tang, J.; Zhou, B., Super Black Material from Low-Density Carbon Aerogels With Subwavelength Structures. *ACS Nano* **2016**, 10, 9123-9128.

(21) Panagiotopoulos, N. T.; Diamanti, E. K.; Koutsokeras, L. E.; Baikousi, M.; Kordatos, E.; Matikas, T. E.; Gournis, D.; Patsalas, P., Nanocomposite Catalysts Producing Durable, Super-Black Carbon Nanotube Systems: Applications in Solar Thermal Harvesting. *ACS Nano* **2012**, 6, 10475-10485.

(22) Han, Z. W.; Wang, Z.; Li, B.; Feng, X. M.; Jiao, Z. B.; Zhang, J. Q.; Zhao, J.; Niu, S. C.; Ren, L. Q., Flexible Self-Cleaning Broadband Antireflective Film Inspired by the Transparent Cicada Wings. *Acs Appl. Mater. Inter.* **2019**, 11, 17019-17027.

(23) Ghai, V.; Singh, H.; Agnihotri, P. K., Ultra-black superhydrophobic multilayer broadband optical absorber. *MRS Adv.* **2019**, *4* (3-4), 163-168.

(24) Zhou, L.; Tan, Y. L.; Wang, J. Y.; Xu, W. C.; Yuan, Y.; Cai, W. S.; Zhu, S. N.; Zhu, J., 3D self-assembly of aluminium nanoparticles for plasmon-enhanced solar desalination. *Nat. Photonics* **2016**, 10, 393.

(25) Zograf, G. P.; Petrov, M. I.; Zuev, D. A.; Dmitriev, P. A.; Milichko, V. A.; Makarov, S. V.; Belov, P. A., Resonant Nonplasmonic Nanoparticles for Efficient Temperature-Feedback Optical Heating. *Nano Lett.* **2017**, 17, 2945-2952.

(26) Chen, X. B.; Liu, L.; Huang, F. Q., Black titanium dioxide (TiO_2) nanomaterials (vol 44, pg 1861, 2015). *Chem. Soc. Rev.* **2015**, 44, 2019-2019.

(27) Sheverdin, A.; Valagiannopoulos, C., Core-shell nanospheres under visible light: Optimal absorption, scattering, and cloaking. *Phys. Rev. B* **2019**, 99,075305..

(28) Azoubel, S.; Cohen, R.; Magdassi, S., Wet deposition of carbon nanotube black coatings for stray light reduction in optical systems. *Surf. Coat. Tech.* **2015**, 262, 21-25.

(29) Bera, R. K.; Mhaisalkar, S. G.; Mandler, D.; Magdassi, S., Formation and performance of highly absorbing solar thermal coating based on carbon nanotubes and boehmite. *Energ. Convers.* Manage. **2016**, 120, 287-293.

(30) Vinetsky, Y.; Jambu, J.; Mandler, D.; Magdassi, S., CNT-Based Solar Thermal Coatings: Absorptance vs. Emittance. *Coatings* **2020**, 10 (11).

(31) Xu, J.; Shi, Y.; Li, J.; Cui, G.; Gu, G., Carbon Aerogel Based Waterborne Ultra-Black Coatings with High Light Absorption. *Coatings* **2021**, *11* (5).

(32) Bychanok, D.; Li, S.; Sanchez-Sanchez, A.; Gorokhov, G., Kuzhir, P., Ogrin, F. Y., Pasc, A.; Ballweg, T.; Mandel, K.; Szczurek, A.; Fierro, V.; Celzard, A., Hollow carbon spheres in microwaves: bio inspired absorbing coating. *Appl. Phys. Lett.* **2016**, 108, 013701.

(33) Pan, L.; Wang, Y.; Xu, H. B.; Ding, Y. B.; Li, Y.; Zhao, J. P., Synthesis of Silica Particles with Precisely Tailored Diameter. Chinese. J. Chem. Phys. **2014**, 27, 563-567.

(34) Li, N.; Zhang, Q.; Liu, J.; Joo, J.; Lee, A.; Gan, Y.; Yin, Y. D., Sol-gel coating of inorganic nanostructures with resorcinol-formaldehyde resin. *Chem. Commun.* **2013**, 49, 5135-5137.

(35) Gil-Herrera, L. K.; Blanco, A.; Juarez, B. H.; Lopez, C., Seeded Synthesis of Monodisperse Core-Shell and Hollow Carbon Spheres. *Small* **2016**, 12, 4357-4362.

(36) Jiang, Q. S.; Li, C.; Shi, S. G.; Zhao, D. G.; Xiong, L.; Wei, H. L.; Yi, L., Assembling ultra-thick and crack-free colloidal crystals via an isothermal heating evaporation induced self-assembly method. *J. Non-Cryst. Solids* **2012**, 358, 1611-1616.

(37) Guo, J.; Li, D.; Qian, Z.; Luo, H.; Yang, M.; Wang, Q.; Xu, J.; Zhao, N., Carbon Vesicles: A Symmetry-Breaking Strategy for Wide-Band and Solvent-Processable Ultrablack Coating Materials. *Adv. Funct. Mater.* **2020**, 30, 1909877.

(38) Valagiannopoulos, C. A.; Alitalo, P., Electromagnetic cloaking of cylindrical objects by multilayer or uniform dielectric claddings. *Phys. Rev. B* **2012**, 85 (11).

ToC Figure

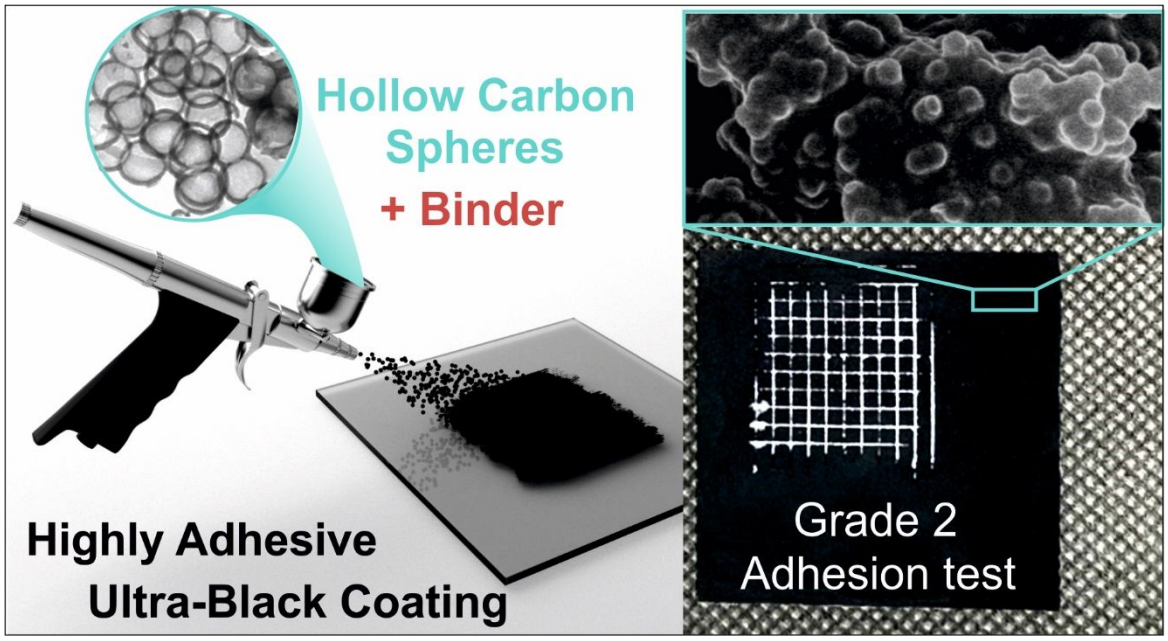
Hollow Carbon Spheres
+ Binder
Highly Adhesive Ultra-Black Coating
Grade 2 Adhesion test